Progress in Fractional Differentiation and Applications
An International Journal

http://dx.doi.org/10.18576/pfda/110304

Analysis of Fractional-Order Model for COVID-19: Implications for Transmission, Hospitalisation, and Recovery Trends

John Olajide Akanni[1,2], *Saheed Ajao*[3] , *Abayomi Ayotunde Ayoade*[4], *Chinwendu Emilian Madubueze*[5] *and Fatmawati Fatmawati*[6,*]

[1] Department of Mathematics, Saveetha School of Engineering, Saveetha Institute of Medical and Technical Sciences, Saveetha University, Chennai 602105, Tamil Nadu, India
[2] Department of Mathematical and Computing Sciences, Koladaisi University, Ibadan, Oyo State, Nigeria
[3] Department of Mathematics and Computer Science, Elizade University, Ondo State, Nigeria
[4] Department of Mathematics, University of Lagos, Akoka, Lagos State, Nigeria
[5] Department of Mathematics, Joseph Sarwuan Tarka University, Makurdi, Benue State, Nigeria
[6] Department of Mathematics, Universitas Airlangga, Kampus C Mulyorejo Surabaya 60115, Indonesia

Received: 2 Nov. 2024, Revised: 18 Dec. 2024, Accepted: 20 Feb. 2025
Published online: 1 Jul. 2025

Abstract: This research uses fractional-order differential equations to explore the dynamics of COVID-19 spread, providing insights into how different parameters influence the epidemic. The study examines how varying fractional order, transmission rates, and recovery rates affect vital metrics such as the number of acute infections, hospitalisations, and other epidemiological factors. Our findings indicate that fractional-order models are adept at capturing complex behaviours, including crossover effects, which are crucial for understanding disease progression. The analysis shows that increasing the transmission rate leads to an increase in acute cases and hospitalisations, highlighting the importance of controlling transmission to reduce the strain on healthcare systems. In addition, higher recovery rates are associated with fewer acute infections, underlining the effectiveness of efficient recovery strategies. The impact of changes in hospitalisation rates and movement dynamics between different infection states on the overall trajectory of the epidemic is also discussed. This research emphasises the utility of fractional-order models in making accurate predictions and guiding public health interventions, ultimately aiding in more informed decision-making and response strategies for managing disease outbreaks.

Keywords: Dynamical system, COVID-19, Stability analysis, Sensitivity analysis, Fractional order, Caputo derivative operator.

1 Introduction

The COVID-19 pandemic, caused by the new coronavirus 2 of severe acute respiratory syndrome (SARS-CoV-2), has emerged as one of the most significant global health challenges in recent history. This virus has caused widespread disruption, including the overwhelming of health systems, significant strains on social relationships, and a marked increase in mental health issues in populations [1]. Initially detected in China at the end of 2019, the virus quickly spread throughout the world, prompting a global health crisis [2]. The pandemic has resulted in millions of deaths and has triggered substantial economic downturns due to global lockdowns and other containment measures [1]. SARS-CoV-2 is transmitted primarily through respiratory droplets expelled when infected individuals talk, cough, or sneeze [3].

Another critical transmission route is through environmental contamination, as the virus can remain viable in the air and on surfaces for varying durations [4]. This means that contact with contaminated surfaces can lead to infection. COVID-19 manifests in a wide range of symptoms, from mild to severe, and can be life-threatening, particularly for older adults and individuals with pre-existing health conditions such as asthma, obesity, hypertension, and diabetes [5]. The most common symptoms include respiratory problems such as shortness of breath, coughing, and fever, with gastrointestinal symptoms such as nausea, vomiting, and diarrhoea also reported [6]. Additional symptoms may include fatigue, loss of

* Corresponding author e-mail: fatmawati@fst.unair.ac.id

taste or smell, muscle pain, sore throat, headaches, and skin rashes. Importantly, many infected individuals may remain asymptomatic, which poses a challenge in controlling the spread of the virus [7,8]. The incubation period for SARS-CoV-2 is typically between two and fourteen days [9]. Genetic studies have shown a high degree of similarity between the virus in humans and related viruses in bats, suggesting a zoonotic origin [10].

Past outbreaks of similar coronaviruses, such as the severe acute respiratory syndrome (SARS) in 2003 and the Middle East respiratory syndrome (MERS) in 2012, have shown similar clinical features, including fever, cough, and difficulty breathing [11,12]. At the end of January 2020, China had reported 571 confirmed cases of COVID-19 [13]. On 30 January 2020, the World Health Organisation (WHO) declared the outbreak a Public Health Emergency of International Concern, and by mid-March 2020, it was classified as a pandemic, having affected more than 334,000 individuals and resulted in approximately 14,500 deaths in more than 190 countries [14]. In June 2023, the WHO estimated that COVID-19 has caused nearly 7 million deaths and more than 768 million confirmed cases worldwide [15].

Fractional-order models incorporate memory and hereditary effects, which are crucial for capturing the temporal dynamics of disease progression. These models account for the fact that a system's current rate of change can depend on its entire history, not just its present state. It is particularly relevant for COVID-19, where infection dynamics and recovery can exhibit delays and lingering effects. Fractional derivatives are inherently nonlocal, meaning that they consider the global behaviour of a system over time. This property allows fractional-order models to better capture the spread of COVID-19 since the disease's transmission depends on cumulative interactions and patterns that evolve, not just instantaneous rates.

Studies have demonstrated that fractional-order models can outperform traditional models in forecasting the trajectory of infectious diseases. They provide better tools for predicting outbreak trends and evaluating control measures, enabling more effective public health responses during pandemics such as COVID-19 [16,17]. By allowing orders of differentiation to be non-integer, fractional-order models provide an additional degree of freedom compared to classical integer-order models. This flexibility enables these models to better fit real-world epidemiological data, especially for diseases with complex transmission patterns such as COVID-19. Fractional-order models have been shown to more accurately represent complex biological and epidemiological systems, including the immune response and the effects of interventions such as vaccination and treatment. These characteristics make them particularly suitable for studying multifaceted diseases such as COVID-19.

Numerous studies have explored the use of integer-order differential equations (IDEs) in modelling the transmission dynamics of infectious diseases [16,17,18,19]. Nonlinear equations, in particular, have provided valuable insights into disease spread, leading to the development of more accurate, data-driven models for COVID-19 [20,21,22,23,24]. For example, Musa *et al.* [25] proposed a compartmental model with eight categories, incorporating public awareness campaigns and hospitalisation strategies to manage COVID-19 transmission in Nigeria. Their findings suggest that inadequate public awareness could lead to increased infection rates. Similarly, Memon *et al.* [26] developed a compartmental SEQIJR model to assess the effectiveness of isolation and quarantine measures in controlling COVID-19 in Pakistan.

Fractional-order differential equations (FODEs) have become powerful tools in modeling complex biological and engineering processes, particularly those with memory effects, which are common in such systems [27,28,29,30]. Unlike integer-order models, which are memoryless, FODEs account for the history of the system, providing a more accurate representation of disease dynamics. For example, patient intervals between doctor visits often follow a power-law distribution, which can be modelled using the Caputo derivative operator (CDO) [31,32,33]. The CDO is particularly advantageous due to its non-local properties and flexibility, which makes it superior to integer-order derivatives in certain applications [34,35,36,37,38].

Given these advantages, the CDO has been widely used in modelling complex problems. For example, Javidi *et al.* [39] extended a mathematical model of the cholera epidemic to include the Caputo derivative. Similarly, other researchers have applied CDO to study the stability of disease models, vector-borne diseases, obesity epidemics, etc. [40,41,42,43,44].

In [45], the authors used a fractional Newton explicit group method to solve time-fractional nonlinear porous medium equations. The implicit finite-difference schemes with the Caputo time-fractional derivative operator were used with this method. The accuracy and efficiency of the fractional Newton explicit group method in solving initial boundary value problems of porous medium equations at different orders of time-fractional derivatives were postulated and discovered that the technique shows more efficacy in solving realistic phenomena. In [46], the article presents a new fractional-order mathematical model for a tumour-immune surveillance mechanism. Baleanu et al. [46] analysed the interactions between various tumour cell populations and the immune system of fractional differential equations (FDEs). They suggested an efficient numerical procedure to solve these FDEs by considering singular and non-singular derivative operators, and an optimal control strategy was employed to study the effect of chemotherapy treatment.

A Caputo-type fractional model was used to study the transmission dynamics of the Nipah virus. The impact of unsafe contact with an infectious corpse as a possible way to transmit this virus was one of the critical factors considered [47]. One of their conclusions was that there should be minimal unsafe contact with the infectious corpse. They also compare fractional and classical results [47]. Similarly, Defteri et al. [48] studied the motion dynamics of an accelerated mass-

spring system within fractional calculus. The Lagrangian and the classical equations of motion using the Euler-Lagrange equations of integer order were constructed to study the system. The generalised Lagrangian was introduced using non-integers, and then the resulting fractional Euler-Lagrange equation was generated and solved numerically.

Recent research has increasingly focused on the application of CDO in epidemic modelling, particularly for COVID-19, due to its ability to accurately capture real-world dynamics in various fields [49,50,51,52]. For example, Baba [53] developed a COVID-19 model using CDO, while another study proposed a SEIQRDP model to analyse the progression of the pandemic [54]. Other researchers have used CDO to examine the impact of lockdowns and other control measures on COVID-19 transmission [55,56,57,58,59,60].

Inspired by the success of FODEs in modelling non-linear real-world systems, this study develops a new deterministic model to explore the dynamics of COVID-19. The model incorporates exposed individuals, acutely infected individuals, infected individuals, recovered individuals, and hospitalised individuals, using Caputo fractional order derivatives. Various simulations are performed to validate the analytical results, and the sensitivity analysis is presented with detailed diagrams. The structure of the paper is as follows: Section 2 outlines the formulation and analysis of the model, Section 3 presents a detailed analysis of the fractional model, Section 4 has the stability and numerical analysis, Section 5 contains the results and discussion, and Section 6 concludes the study.

2 Model formulation and analysis

In this section model formulation and analysis are presented in chronological order.

2.1 Model formulation

We consider a total human population $N(t)$ at time t, which is divided into six distinct compartments: susceptible individuals $S(t)$, exposed individuals $E(t)$, acutely infected individuals $A(t)$, infected individuals $I(t)$, hospitalized individuals $H(t)$, and recovered individuals $R(t)$. The total population is represented by the equation:

$$N(t) = S(t) + E(t) + A(t) + I(t) + H(t) + R(t). \tag{1}$$

The susceptible population $S(t)$ increases as new individuals enter the population at a rate Λ, assuming these individuals are initially susceptible. However, this population decreases as individuals become exposed to the infection at a rate proportional to $\frac{\beta(I(t)+\eta A(t))}{N(t)}S(t)$, where β represents the infection rate, and η adjusts for the relative infectiousness of acutely infected individuals compared to those in the infected class. The exposed population $E(t)$ consists of individuals who have been infected but are not yet infectious. Individuals enter this compartment at the same rate $\frac{\beta(I(t)+\eta A(t))}{N(t)}S(t)$. The number of exposed individuals decreases as they progress to either the acutely infected compartment $A(t)$ at a rate ε, or to the infected compartment $I(t)$ at a rate θ. The acutely infected population $A(t)$ increases as individuals move from the exposed class $E(t)$ at a rate ε. This population then decreases as individuals progress to the infected class $I(t)$ at a rate ψ, to the hospitalized class $H(t)$ at a rate ϕ, or recover to the recovered class $R(t)$ at a rate κ. The infected population $I(t)$ increases as individuals progress from the exposed class $E(t)$ at a rate θ and from the acutely infected class $A(t)$ at a rate ψ. This population decreases as individuals are hospitalized at a rate ω, or die from the disease at a rate δ. The hospitalized population $H(t)$ grows as individuals move from the acutely infected class $A(t)$ at a rate ϕ and from the infected class $I(t)$ at a rate ω. This population decreases due to recovery at a rate ρ or due to disease-induced mortality at a rate δ. Finally, the recovered population $R(t)$ increases as individuals recover from the acutely infected class $A(t)$ at a rate κ and from the hospitalized class $H(t)$ at a rate ρ. The recovered population decreases due to natural death at a rate

μ. The dynamics of the model are governed by the following system of differential equations:

$$\begin{aligned}
\frac{dS(t)}{dt} &= \Lambda - \frac{\beta(I(t)+\eta A(t))}{N(t)}S(t) - \mu S(t),\\
\frac{dE(t)}{dt} &= \frac{\beta(I(t)+\eta A(t))}{N(t)}S(t) - (\varepsilon+\theta+\mu)E(t),\\
\frac{dA(t)}{dt} &= \varepsilon E(t) - (\psi+\phi+\kappa+\mu)A(t),\\
\frac{dI(t)}{dt} &= \theta E(t) + \psi A(t) - (\omega+\delta+\mu)I(t),\\
\frac{dH(t)}{dt} &= \phi A(t) + \omega I(t) - (\rho+\delta+\mu)H(t),\\
\frac{dR(t)}{dt} &= \kappa A(t) + \rho H(t) - \mu R(t).
\end{aligned} \tag{2}$$

These equations describe the transitions between the compartments, capturing the overall dynamics of disease transmission and progression within the population.

Table 1: Definition of variables of model (2)

Parameter	Variable
S	Susceptible class
E	Exposed class
A	Acutely COVID-19-infected class
I	Infected class
H	Hospitalized class
R	Recovered class

Table 2: Definition of parameters in the model (2)

Parameter	Description
Λ	Stable enrollment rate
β	COVID-19 transmission probability
η	Modification parameter for A
μ	Natural mortality rate
ε	Rate of movement from E to A
θ	Rate of movement from E to I
ψ	Rate of movement from A to I
ϕ	Hospitalize rate of A
κ	Recovery rate of A
δ	Induced death rate
ω	Hospitalize rate of I
ρ	Recovery Rate of H

For computational convenience, we let

$$C_1 = \varepsilon+\theta+\mu, \qquad C_2 = \mu+\psi+\phi+\kappa,$$
$$C_3 = \mu+\delta+\omega, \qquad C_4 = \mu+\delta+\rho,$$
$$\lambda = \frac{\beta(I(t)+\eta A(t))}{N(t)}.$$

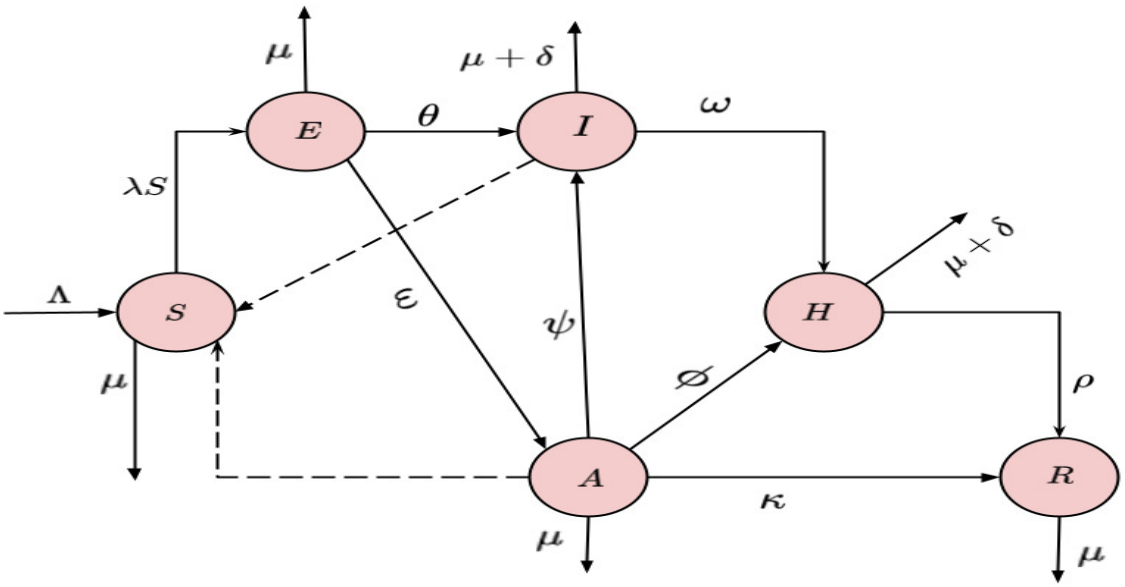

Fig. 1: Flow chart of the model where λ is given in (2)

Then, the equations of model (2) become

$$\begin{aligned}
\frac{dS}{dt} &= \Lambda - (\lambda + \mu)S, \\
\frac{dE}{dt} &= \lambda S - C_1 E, \\
\frac{dA}{dt} &= \varepsilon E - C_2 A, \\
\frac{dI}{dt} &= \theta E + \psi A - C_3 I, \\
\frac{dH}{dt} &= \phi A + \omega I - C_4 H, \\
\frac{dR}{dt} &= \kappa A + \rho H - \mu R.
\end{aligned} \tag{3}$$

2.2 Basic Properties

We explore the fundamental properties of the model here. This section explores the essential characteristics of the model.

2.2.1 Positivity of Solutions

Theorem 1. *Given the initial conditions $S(0) > 0$, $E(0) > 0$, $A(0) > 0$, $I(0) > 0$, $H(0) > 0$, and $R(0) > 0$, the solutions $S(t)$, $E(t)$, $A(t)$, $I(t)$, $H(t)$, and $R(t)$ of the model (2) will remain positive for all $t > 0$.*

Proof. Let $t_1 = \sup\{t > 0 : S(t) > 0, E(t) > 0, A(t) > 0, I(t) > 0, H(t) > 0, R(t) > 0\}$, where $t_1 > 0$. From the first equation in the model:

$$\frac{dS}{dt} = \Lambda - (\lambda + \mu)S, \tag{4}$$

we have:

$$\frac{dS}{dt} \geq -(\lambda+\mu)S. \tag{5}$$

Integrating both sides over the interval $[0,t_1]$, we obtain:

$$\int_0^{t_1} \frac{dS}{S(t)} \geq \int_0^{t_1} -(\lambda+\mu)dt, \tag{6}$$

which leads to:

$$S(t_1) \geq S(0)e^{-\mu t_1 - \int_0^{t_1} \lambda(\tau)d\tau} \geq 0 \quad \text{as} \quad t_1 \to \infty. \tag{7}$$

Using a similar approach, it can be shown that $E(t) > 0$, $A(t) > 0$, $I(t) > 0$, $H(t) > 0$, and $R(t) > 0$ for all $t > 0$. This completes the proof.

2.2.2 Invariant Region

Theorem 2.*Assume that the model (2) describes the system with solutions $S(t)$, $E(t)$, $A(t)$, $I(t)$, $H(t)$, and $R(t)$. If the initial values $S(0)$, $E(0)$, $A(0)$, $I(0)$, $H(0)$, and $R(0)$ are positive, then for all $t > 0$, the system remains within the region defined by:*

$$D = \left\{ (S,E,A,I,H,R) \in \mathbb{R}_+^6 : N \leq \frac{\Lambda}{\mu} \right\}. \tag{8}$$

This region is positively invariant under the dynamics of the model.

*Proof.*Following the approach outlined in [61], summing all the compartments in (2) yields:

$$\frac{dN}{dt} = \Lambda - \mu N - \delta(I+H). \tag{9}$$

This simplifies to:

$$\frac{dN}{dt} \leq \Lambda - \mu N. \tag{10}$$

Thus, we have:

$$N(t) \leq N(0)e^{-\mu t} + \frac{\Lambda}{\mu}(1-e^{-\mu t}). \tag{11}$$

If $N(0) \leq \frac{\Lambda}{\mu}$, it follows that $N(t) \leq \frac{\Lambda}{\mu}$. Therefore, the solution remains within the region D for all $t > 0$, indicating that D is a positively invariant set. Consequently, the dynamics of the model can be analysed within D.

2.3 Disease-Free Equilibrium and Basic Reproduction Number

In the absence of infection, the disease-free equilibrium, denoted by E^o, is given by:

$$E^o = (S^0,E^0,A^0,I^0,H^0,R^0) = \left(\frac{\Lambda}{\mu},0,0,0,0,0\right). \tag{12}$$

The basic reproduction number, R_0, is a critical epidemiological metric that indicates whether an infection will decline or persist within a population. Defined as the expected number of secondary infections produced by a single infected individual in a fully susceptible population [62], R_0 is expressed as:

$$R_0 = \frac{\beta(\eta\varepsilon C_3 + \psi\varepsilon + \theta C_2)}{C_3C_2C_1}. \tag{13}$$

Here, R_0 quantifies the average number of new infections caused by a COVID-19-infected individual among susceptible individuals. Based on Theorem 2 from [63], the following result is established:

Lemma 1.*The disease-free equilibrium of the model (2) is locally asymptotically stable if $R_0 < 1$ and unstable if $R_0 > 1$.*

This lemma suggests that COVID-19 can be eradicated if the initial population size is within the basin of attraction of the disease-free equilibrium.

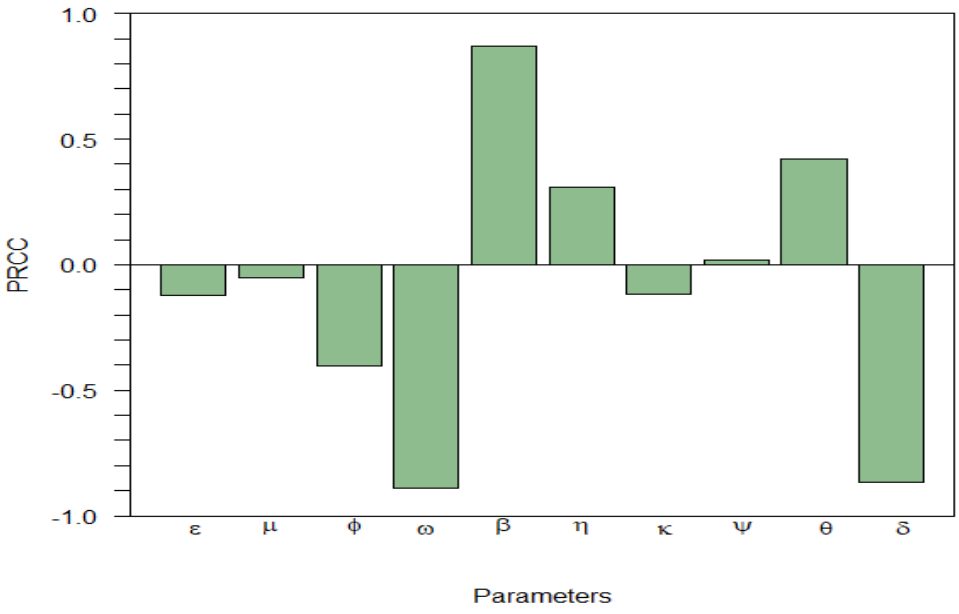

Fig. 2: Partial Rank Correlation Coefficient plots of different parameters of model (2) using basic reproduction number R_0 as the response function

2.4 Endemic Equilibrium

We explore the equilibrium in which the disease is present. Let the endemic equilibrium of the model be denoted by $E_1 = (S^*, E^*, A^*, I^*, H^*, R^*)$. Then, solving the model equations (3) at steady state, we have

$$\begin{aligned}
S^* &= \frac{\pi}{\lambda^* + \mu}, \\
E^* &= \frac{\lambda^* \pi}{C_1(\lambda^* + \mu)}, \\
A^* &= \frac{\varepsilon \lambda^* \pi}{C_1 C_2(\lambda^* + \mu)}, \\
I^* &= \frac{(C_2\theta + \psi\varepsilon)\lambda^* \pi}{C_1 C_2 C_3(\lambda^* + \mu)}, \\
H^* &= \frac{[C_3\phi\varepsilon + \omega(C_2\theta + \psi\varepsilon)]\lambda^* \pi}{C_1 C_2 C_3 C_4(\lambda^* + \mu)}, \\
R^* &= \frac{\left[C_3 C_4 \kappa\varepsilon + \rho[C_3\phi\varepsilon + \omega(C_2\theta + \psi\varepsilon)]\right]\lambda^* \pi}{C_1 C_2 C_3 C_4(\lambda^* + \mu)}.
\end{aligned} \tag{14}$$

Let the force of infection at the endemic state be denoted by λ^* and it is given by

$$\lambda^* = \frac{\beta(I^* + \eta A^*)}{N^*}. \tag{15}$$

Substituting (14) into (15) leads to

$$P_1 \lambda^{*2} + P_2 \lambda^* + P_3 = 0, \tag{16}$$

where

$$P_1 = C_2C_3C_4\mu + C_3C_4\varepsilon\mu + C_4\mu(C_2\theta + \psi\varepsilon) + \mu\left[C_3\phi\varepsilon + \omega(C_2\theta + \psi\varepsilon)\right] + \left[C_3C_4\kappa\varepsilon + \rho[C_3\phi\varepsilon + \omega(C_2\theta + \psi\varepsilon)]\right], \tag{17}$$

$$P_2 = \mu[P_1 + (1-R_0)C_1C_2C_3C_4], \tag{18}$$

$$P_3 = (1-R_0)C_1C_2C_3C_4\mu^2. \tag{19}$$

From (16), $P_1 > 0$, $P_3 > 0$ if $R_0 < 1$ and $P_3 < 0$ if $R_0 > 1$. Hence, the following result is obtained:

Theorem 3. *The COVID-19 model (2) has*

1.one unique endemic equilibrium if $P_3 < 0$ (Corresponding to when $R_0 > 1$)
2.one unique endemic equilibrium if $P_2 < 0$ and $P_3 = 0$ or ${P_2}^2 - 4P_1P_3 = 0$
3.two unique endemic equilibria if $P_3 > 0$ and $P_2 < 0$ and ${P_2}^2 - 4P_1P_3 > 0$
4.none otherwise

2.5 Global Stability of Endemic Equilibrium

We try to prove the global asymptotic stability of the endemic equilibrium of the model with $\theta = \phi = 0$, and $\delta = 0$. The model has the endemic equilibrium given by

$$E_1 = (S^*, E^*, A^*, I^*, H^*, R^*). \tag{20}$$

By assuming $\delta = 0$, the total population $N \to \frac{\Lambda}{\mu}$ as $t \to \infty$ and so doing, the force of infection reduces to

$$\lambda = \hat{\beta}(I + \eta A), \tag{21}$$

where

$$\hat{\beta} = \frac{\beta\mu}{\Lambda}.$$

Let the associated reproduction number of the model be $\hat{R_0} = R_{0|\theta=\phi=\delta=0}$

Theorem 4. *Consider the COVID-19 model (2) with $\theta = \phi = 0$. The endemic equilibrium E_1 is globally asymptotically stable in $D\backslash D_o$ whenever $\hat{R_0} > 1$, where*

$$D_o = \{(S, E, A, I, H, R) \in D : E = A = I = H = R = 0\}.$$

Proof. Consider the COVID-19 model (2) having $\theta = \phi = 0$ with (21) and $\hat{R_0} > 1$. We use the Lyapunov function given as thus:

$$L = S - S^* - S^* ln\frac{S}{S^*} + E - E^* - E^* ln\frac{E}{E^*} + X\left[A - A^* - A^* ln\frac{A}{A^*}\right] + Y\left[I - I^* - I^* ln\frac{I}{I^*}\right] + Z\left[H - H^* - H^* ln\frac{H}{H^*}\right]. \tag{22}$$

Taking the time derivative of (22) leads to

$$L' = S' - \frac{S^*}{S}S' + E' - \frac{E^*}{E}E' + X\left[A' - \frac{A^*}{A}A'\right] + Y\left[I' - \frac{I^*}{I}I'\right] + Z\left[H' - \frac{H^*}{H}H'\right], \tag{23}$$

where

$$X = \frac{C_1}{\varepsilon}, \tag{24}$$

$$Y = \frac{C_1C_2 - \hat{\beta}S\eta\varepsilon}{\varepsilon\psi}, \tag{25}$$

$$Z = \frac{C_1C_2C_3 - \hat{\beta}S\eta\varepsilon C_3 - \hat{\beta}S\varepsilon\psi}{\varepsilon\omega\psi}. \tag{26}$$

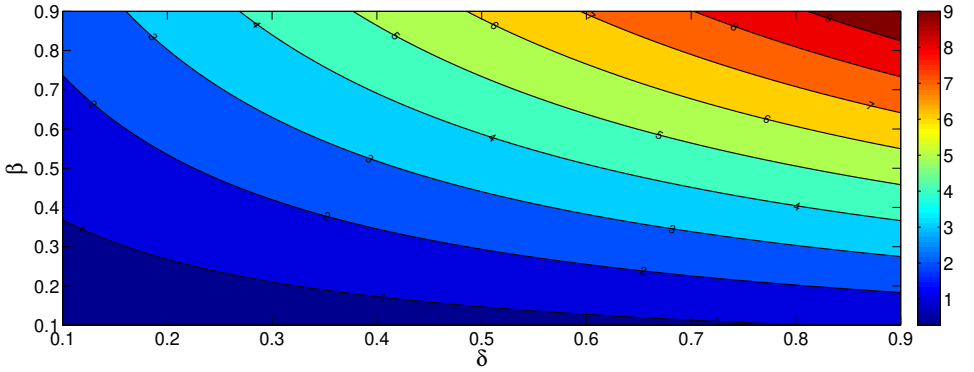

Contour plot of $\mathscr{R}_0$ as a function of β and δ

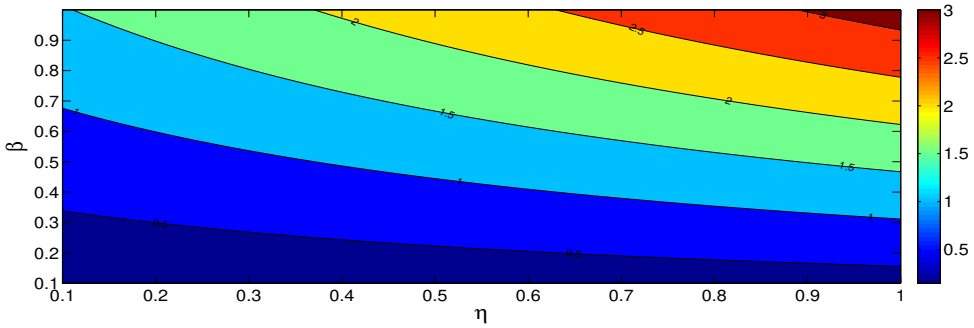

Contour plot of $\mathscr{R}_0$ as a function of β and η

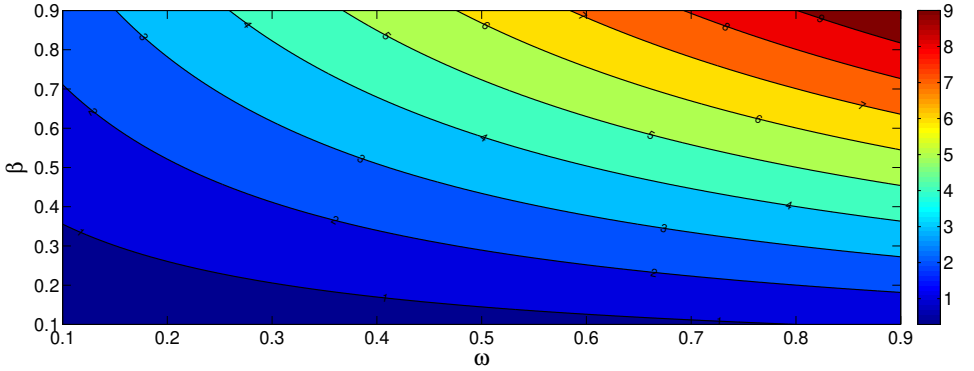

Contour plot of $\mathscr{R}_0$ as a function of β and ω

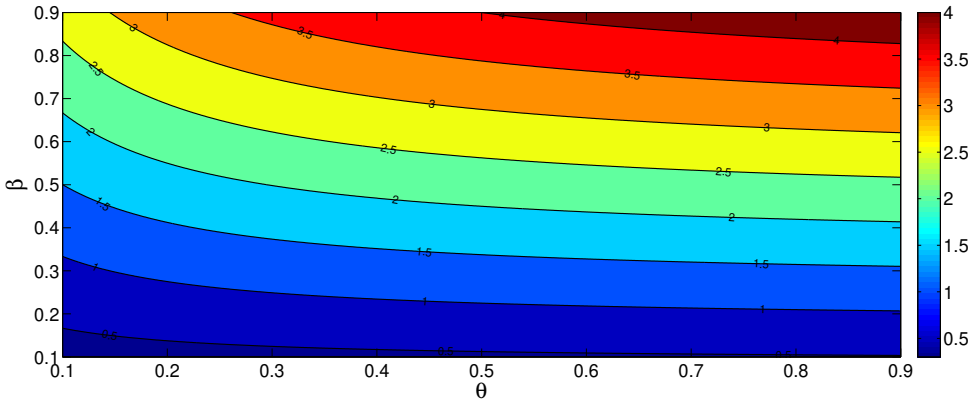

Contour plot of $\mathscr{R}_0$ as a function of β and θ

Fig. 3: 2-D contour plots of the control reproduction number, R_0

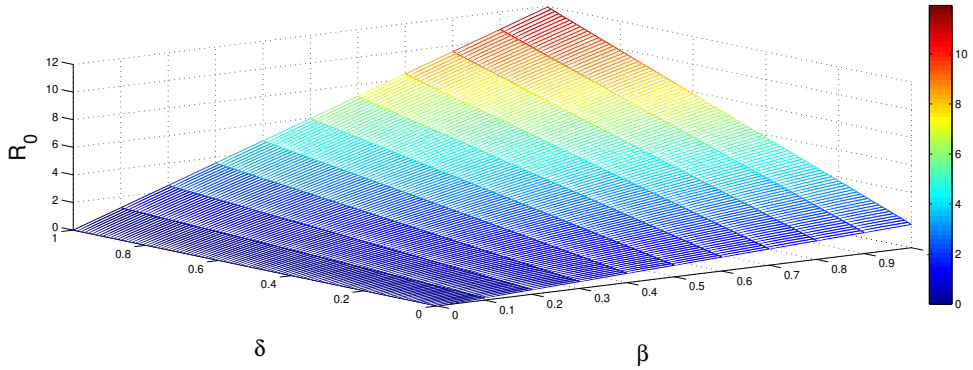

3-D Contour plot of $\mathscr{R}_0$ as a function of β and δ

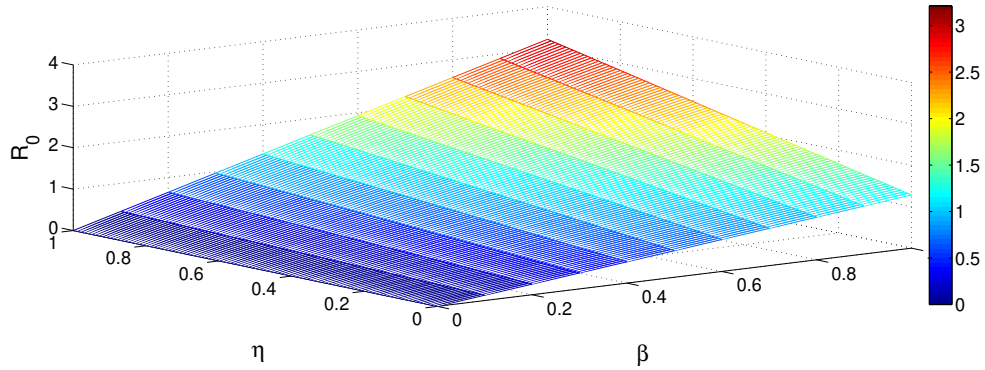

3-D Contour plot of $\mathscr{R}_0$ as a function of β and η

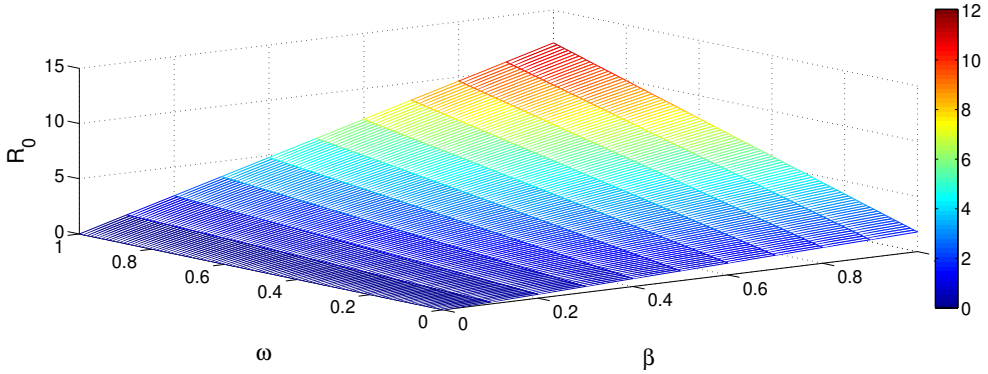

3-D Contour plot of $\mathscr{R}_0$ as a function of β and ω

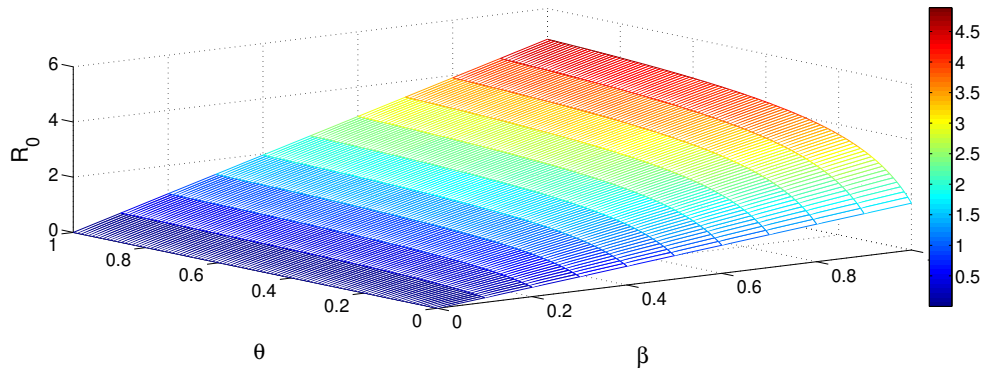

3-D Contour plot of $\mathscr{R}_0$ as a function of β and θ

Fig. 4: 3-D contour plots of the control reproduction number, $\mathscr{R}_0$

With $\Lambda = \hat{\beta}(I^* + \eta A^*)S^* + \mu S^*$, (23) becomes

$$\begin{aligned} L' &= \hat{\beta}(I^* + \eta A^*)S^* + \mu S^* - \mu S - \left[\frac{\hat{\beta}(I^* + \eta A^*)S^{*2}}{S} + \frac{\mu S^{*2}}{S} - \hat{\beta}(I^* + \eta A^*)S^* - \mu S^*\right] \\ &- C_1 E - \frac{\hat{\beta}(I + \eta A)SE^*}{E} + C_1 E^* + \frac{C_1}{\varepsilon}\left[\varepsilon E - C_2 A - \frac{\varepsilon E A^*}{A} + C_2 A^*\right] \\ &+ \frac{C_1 C_2 - \hat{\beta} S\eta\varepsilon}{\varepsilon\psi}\left[\psi A - C_3 - \frac{\psi A I*}{I} + C_3 I^*\right] + \frac{C_1 C_2 C_3 - \hat{\beta} S\eta\varepsilon C_3 - \hat{\beta} S\varepsilon\psi}{\varepsilon\omega\psi} \\ &\times \left[\omega I - C_4 H - \frac{\omega I H^*}{H} + C_4 H\right]. \end{aligned} \tag{27}$$

Further simplification with

$$C_1 = \frac{\hat{\beta}(I^* + \eta A^*)S^*}{E^*}, \qquad C_2 = \frac{\varepsilon E^*}{A^*}, \qquad C_3 = \frac{\psi A^*}{I^*}, \qquad C_4 = \frac{\omega I^*}{H^*}, \tag{28}$$

leads to

$$\begin{aligned} L' &= 3\hat{\beta}(I^* + \eta A^*)S^* + \mu S^* - \mu S - \frac{\hat{\beta}(I^* + \eta A^*)S^{*2}}{S} - \frac{\mu S^{*2}}{S} + \mu S^* - \frac{\hat{\beta}(I + \eta A)SE^*}{E} \\ &- \frac{\hat{\beta}(I^* + \eta A^*)S^* EA^*}{E^* A} - \frac{\hat{\beta} I^{*2} AS^*}{A^* I} + \hat{\beta} I^* S^*. \end{aligned} \tag{29}$$

Then,

$$\begin{aligned} L' &= \hat{\beta} I^* S^*\left(4 - \frac{S^*}{S} - \frac{SIE^*}{S^* I^* E} - \frac{EA^*}{E^* A} - \frac{AI^*}{A^* I}\right) + \mu S^*\left(2 - \frac{S^*}{S} - \frac{S}{S^*}\right) \\ &+ \hat{\beta}\eta A^* S^*\left(3 - \frac{S^*}{S} - \frac{SAE^*}{S^* A^* E} - \frac{EA^*}{E^* A}\right). \end{aligned} \tag{30}$$

With the arithmetic mean greater than the geometric mean, we have the following inequalities:

$$4 - \frac{S^*}{S} - \frac{SIE^*}{S^* I^* E} - \frac{EA^*}{E^* A} - \frac{AI^*}{A^* I} \le 0, \qquad 2 - \frac{S^*}{S} - \frac{S}{S^*} \le 0, \qquad 3 - \frac{S^*}{S} - \frac{SAE^*}{S^* A^* E} - \frac{EA^*}{E^* A} \le 0.$$

Therefore, $L' \le 0$ for $\hat{R_0} > 1$. Hence, L' is a Lyapunov function in $D\backslash D_o$, and by LaSalle's Invariance Principle [64], every solution of the model with the initial conditions in $D\backslash D_o$ approaches the associated endemic equilibrium E_1 as $t \to \infty$ whenever $\hat{R_0} > 1$.

2.6 Sensitivity Analysis

A global sensitivity analysis is performed using Latin hypercube sampling (LHS) and partial rank correlation coefficients (PRCC) to determine the parameters that most significantly affect model (2) fluctuation with respect to the basic reproduction number R_0, provided in (13). By assuming that every model parameter follows a uniform distribution, LHS matrices are produced. Then, a number of runs with 1000 samples are performed based on the baseline values for the model parameters listed in Table 3. This is done using an approach identical to that of the researchers in [65,66]. The PRCC between each parameter and $\mathscr{R}_0$ is then determined, which allows us to assess the sensitivity of the model parameters.

In Figure 2 and Table 4, the PRCC values for each of the model's sensitive parameters are presented, for those parameters with positive, they have a positive relationship (β,η, ψ and θ), and negative for others, similarly have a negative relationship (μ, ε, ϕ, ω, κ and δ). The results in Figures 3 and 4 support the outcome of the global sensitivity analysis presented in Figure 2 and Table 4.

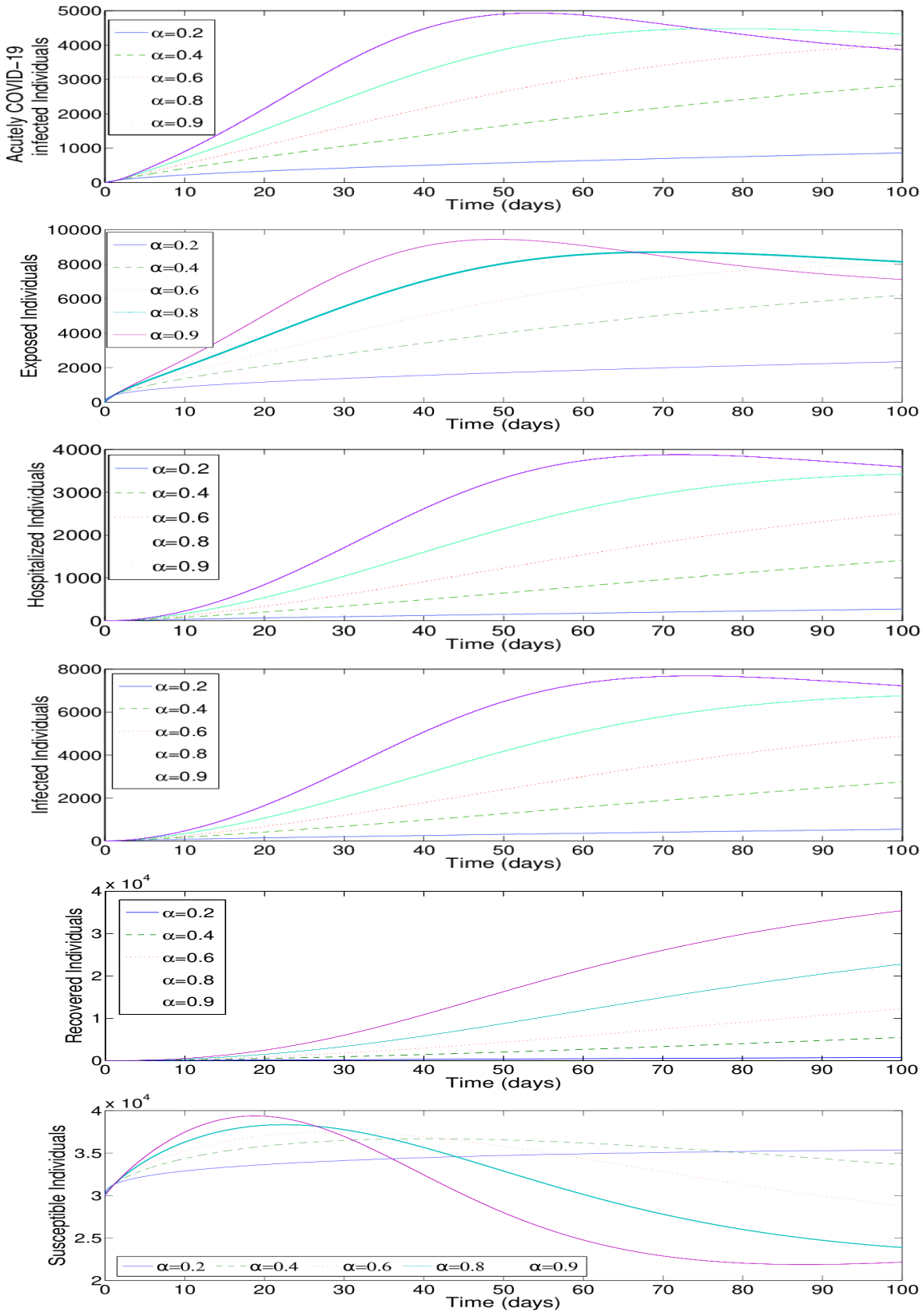

Fig. 5: Fractional dynamics of different classes : (a) A, (b) E, (c) H, (d) I, (e) R, (f) S for different fractional order α

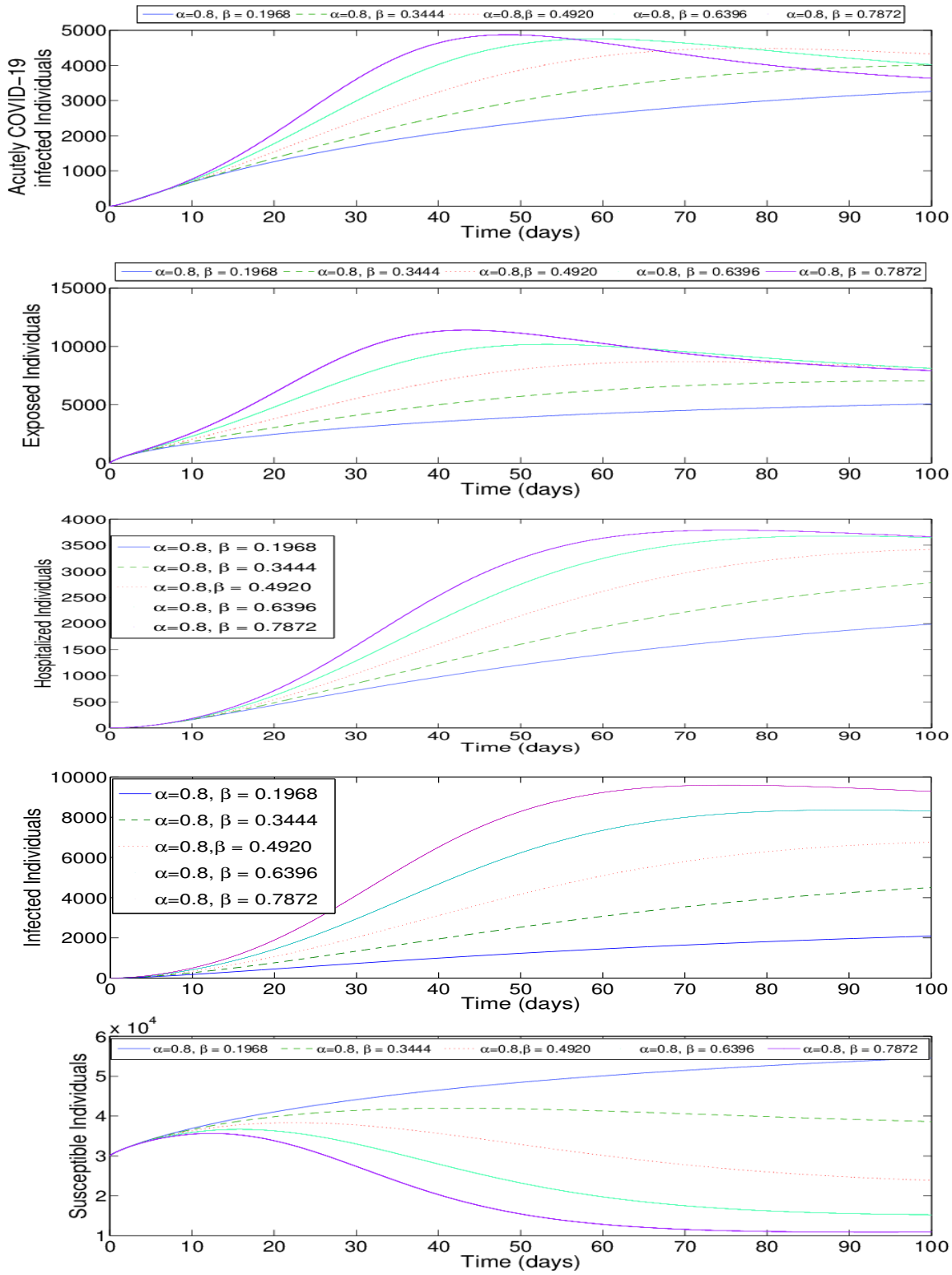

Fig. 6: Fractional dynamics with a Fractional order, $\alpha = 0.8$, while the COVID-19 transmission rate is varied on (a) A, (b) E, (c) H, (d) I, (e) S

Table 3: Values of the parameters used in model (2)

Parameter	Baseline value	Range	Source
β	0.492	0.002-0.75	[69]
η	0.4	0-1	Assumed
μ	0.01277	0.0107-0.0148	[66]
ε	0.18	0.098-0.278	[71]
θ	0.02	0.009-0.4	Assumed
ψ	0.1	0.05-0.5	[67]
δ	0.036	0.01-0.06	[69]
Λ	1500	500-3500	[72]
ρ	0.096	0.0625-0.125	[73]
ω	0.0264	0.0059-0.0679	[65]
ϕ	0.083	0.04-0.2	[68]
κ	0.13978	0.033-0.333	[70]

Table 4: PRCC Values

Parameter	PRCC value	Parameter	PRCC value
β	0.9614	η	0.1439
μ	-0.0610	ε	-0.1566
θ	0.5005	ψ	0.3626
ω	-0.7102	ϕ	-0.1504
κ	-0.2047	δ	-0.6221

3 Analysis of the Fractional Model

3.1 Fundamental Concepts in Fractional Calculus

This section introduces some fundamental concepts in fractional calculus, specifically within the framework of Caputo derivatives.

Definition 1 According to [74], if y is a function in $\mathscr{C}^m$, where m is a natural number, then the Caputo derivative of order κ in the interval $(m-1,m)$ is defined as:

$$ {}^{C}D_t^{\kappa}(p(t)) = \frac{1}{\Gamma(m-\kappa)} \int_0^t (t-s)^{m-\kappa-1} p^{(m)}(s)\, ds, \tag{31} $$

where $\Gamma(\cdot)$ denotes the Gamma function. As κ approaches 1, ${}^{C}D_t^{\kappa}(p(t))$ converges to the first derivative $p'(t)$.

Definition 2 As detailed in [74], the fractional integral of a function $p : \mathbb{R}^+ \to \mathbb{R}$ with order $\kappa > 0$ is given by:

$$ I_x^{\kappa}(p(x)) = \frac{1}{\Gamma(\kappa)} \int_0^x (x-s)^{\kappa-1} p(s)\, ds, \quad 0 < \kappa < 1, \quad x > 0. \tag{32} $$

Definition 3 Let y^* represent the equilibrium of the Caputo fractional model. The Caputo fractional derivative is given by:

$$ {}^{C}D_t^{\kappa}(p(x)) = h(x,p(x)), \quad \text{where} \quad \kappa \in (0,1), \quad \text{if and only if} \quad h(x,p^*) = 0. \tag{33} $$

The Caputo fractional model describing the transmission of COVID-19 is represented as follows:

$$ \begin{aligned} {}^{C}D_t^{\alpha} S(t) &= \Lambda^{\alpha} - (\lambda^{\alpha} + \mu^{\alpha}) S(t), \\ {}^{C}D_t^{\alpha} E(t) &= \lambda^{\alpha} S(t) - (\varepsilon^{\alpha} + \theta^{\alpha} + \mu^{\alpha}) E(t), \\ {}^{C}D_t^{\alpha} A(t) &= \varepsilon^{\alpha} E(t) - (\mu^{\alpha} + \psi^{\alpha} + \phi^{\alpha} + \kappa^{\alpha}) A(t), \\ {}^{C}D_t^{\alpha} I(t) &= \theta^{\alpha} E(t) + \psi^{\alpha} A(t) - (\mu^{\alpha} + \delta^{\alpha} + \omega^{\alpha}) I(t), \\ {}^{C}D_t^{\alpha} H(t) &= \phi^{\alpha} A(t) + \omega^{\alpha} I(t) - (\mu^{\alpha} + \delta^{\alpha} + \rho^{\alpha}) H(t), \\ {}^{C}D_t^{\alpha} R(t) &= \kappa^{\alpha} A(t) + \rho^{\alpha} H(t) - \mu^{\alpha} R(t), \end{aligned} \tag{34} $$

where $S(t) > 0$, $E(t) \geq 0$, $A(t) \geq 0$, $I(t) \geq 0$, $H(t) \geq 0$, and $R(t) \geq 0$.

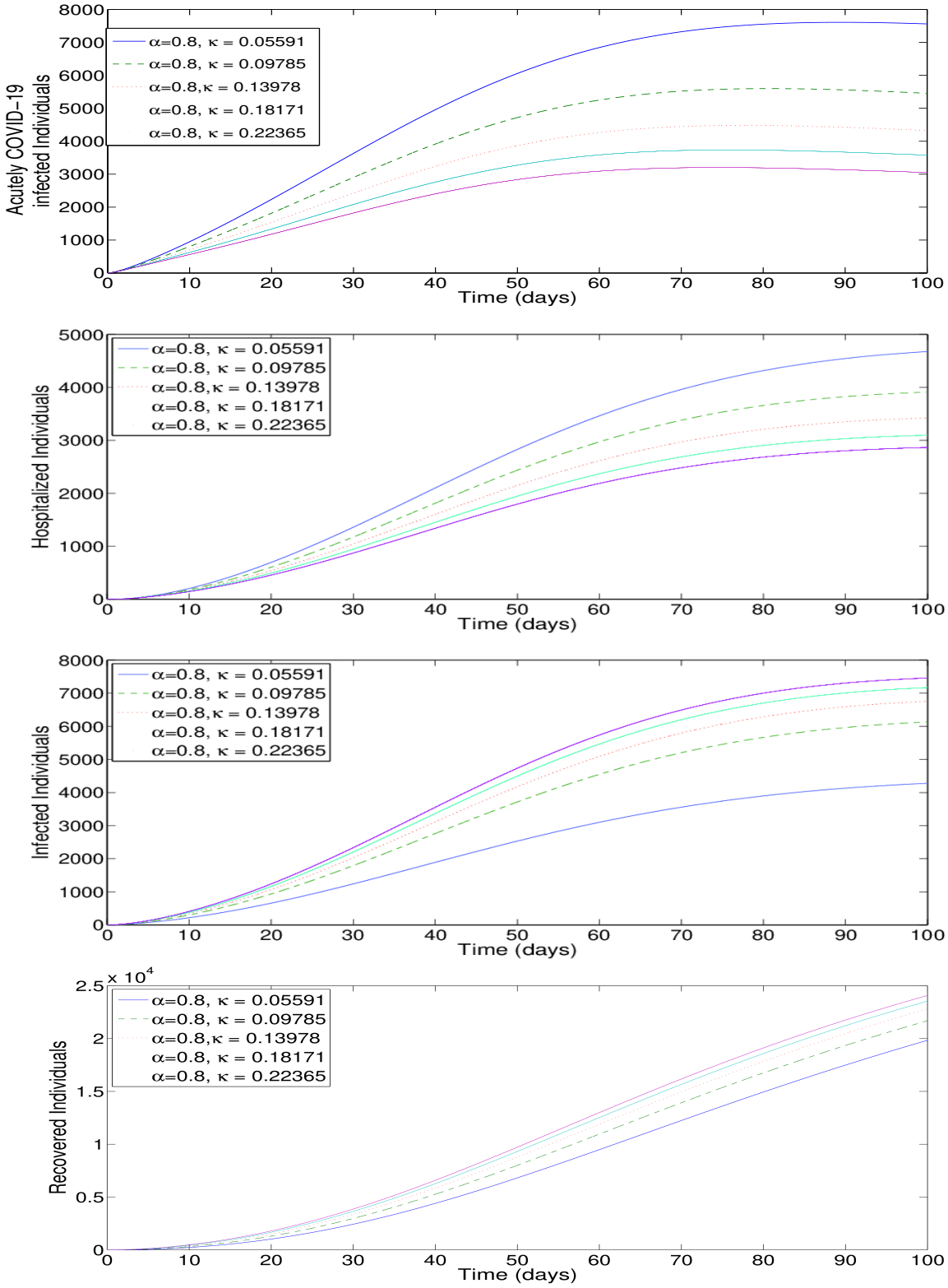

Fig. 7: Fractional dynamics illustrating the impact of varying the recovery rate of A with a fractional order of $\alpha = 0.8$ on (a) A, (b) H, (c) I, (d) R.

3.2 Criteria for the Validity of the Fractional Model

The legitimacy of the fractional model is determined based on several criteria including non-negativity and uniform boundedness, and Hyers-Ulam stability.

3.2.1 Non-negativity and Uniform Boundedness

Let

$$\Omega = \left\{ N(t) : N(t) = (S(t), E(t), A(t), I(t), H(t), R(t)) \in \mathbb{R}_+^6; N(t) \geq 0 \right\}.$$

Theorem 5. *Consider a function $m(x) \in C[u,v]$ where ${}^C D_x^\alpha \in C(u,v]$ with $0 < \alpha \leq 1$. Then, it follows that*

$$m(x) = m(x) + \frac{1}{\Gamma(\alpha)} ({}^C D_x^\alpha n)(\varepsilon)(x-u)^\alpha, \tag{35}$$

provided $u \leq \varepsilon \leq x$, for all $x \in (u,v]$.

We will use the principles outlined in [75,76] to demonstrate that all positive solutions to the model remain within the set Ω using Theorem (5).

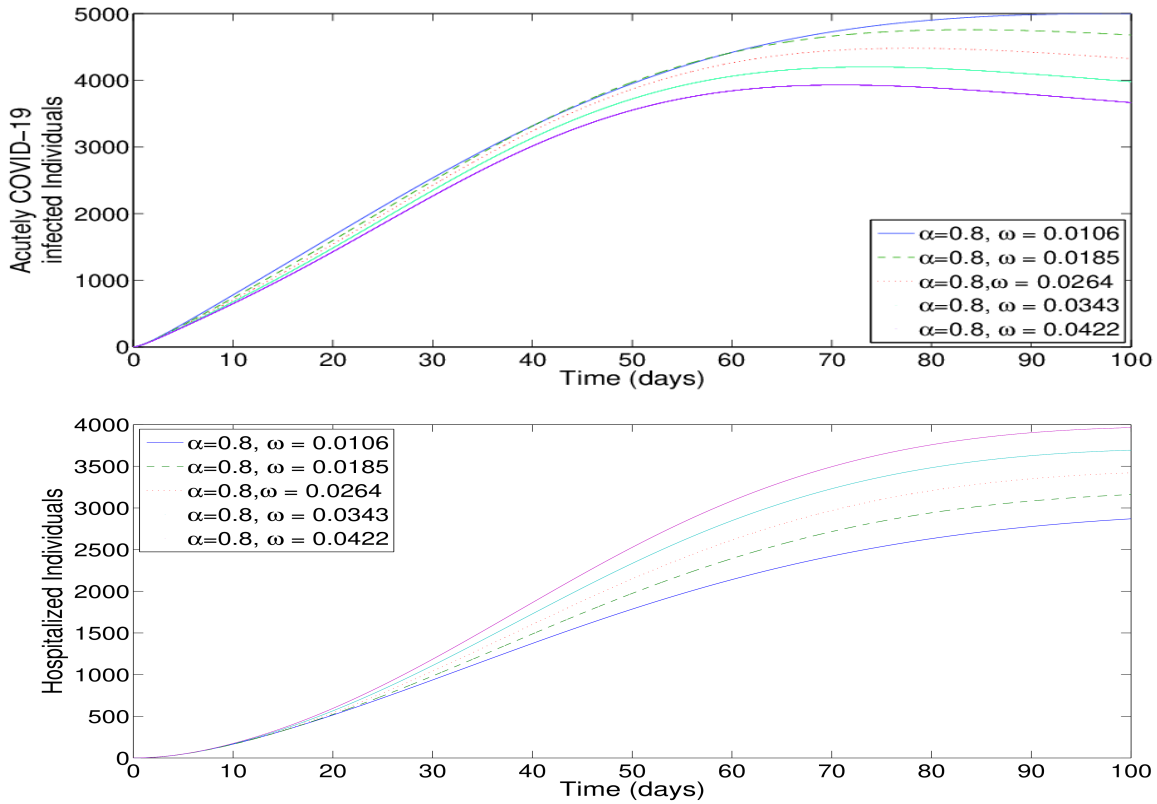

Fig. 8: Fractional dynamics showing variations in the hospitalization rate of I with a fractional order $\alpha = 0.8$ on (a) A, (b) H.

Corollary 1. *Let $n(x) \in [u,v]$ with ${}_0^C D_x^\alpha \in (u,v]$ and $0 < \alpha \leq 1$. If ${}_0^C D_x^\alpha n(0) \geq 0$ for all $t \in (0,v)$, then the function n decreases for all $x \in (0,v)$.*

Theorem 6. *The solution to the COVID-19 model (34) remains positive within the set Ω.*

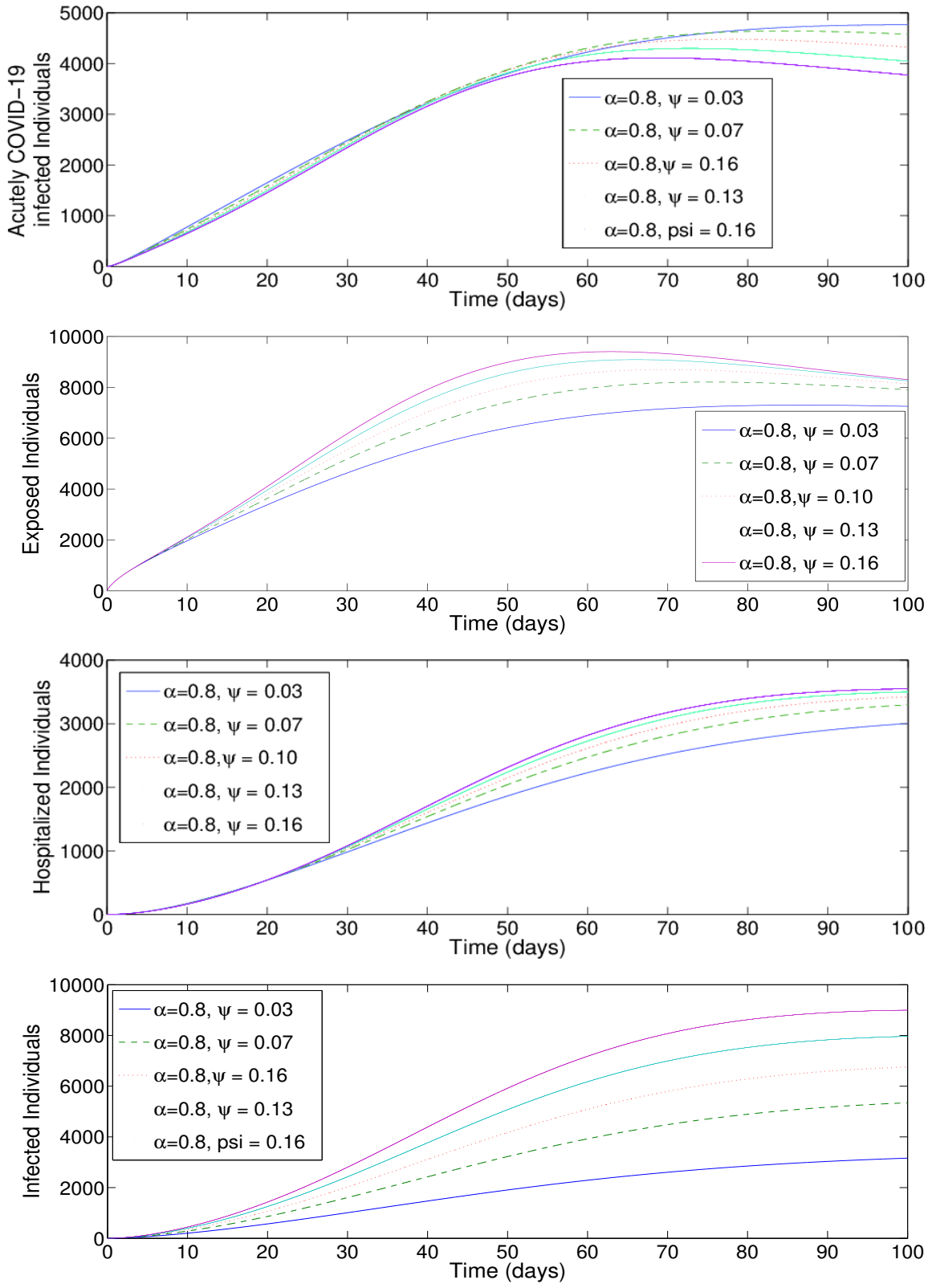

Fig. 9: Dynamics of the fractional model illustrating progression rate from A to I with a fractional order $\alpha = 0.8$ on (a) A, (b) E, (c) H, (d) I.

4 Stability and Numerical Analysis

To substantiate the proposed model described in Equation (34), we provide a series of theoretical results and solutions.

Theorem:

Consider a Banach space denoted by $(\mathscr{B}, \|\cdot\|)$, and let X^* represent a self-map on $\mathscr{B}$. The recursive relation is expressed as $z_{n+1} = x(X^*, z_n)$, and the fixed point of X^* is denoted by $\mathscr{C}(X^*)$. By definition, we can analyse $\|y^*_{n+1} - x(X^*, y^*_n)\|$ within the set $\{y^*_n \subseteq \mathscr{B}\}$. If $\lim_{n\to\infty} C_n = 0$, which means that $\lim_{n\to\infty} C^*_n = p^*$ for $z_{n+1} = X^*$ and n represents the Picard iteration, then the iteration at X^* is stable. The theorem is summarised as follows: Let $(\mathscr{B}, \|\cdot\|)$ be a Banach space, and X^* be a self-map on $\mathscr{B}$. For all $x, y \in \mathscr{B}$, the following holds:

$$
\begin{aligned}
S_{n+1}(t) &= S_n(t) + \mathscr{L}^{-1}\left\{\frac{1}{S^a}\mathscr{L}\{\Lambda^\alpha - (\lambda^\alpha + \mu^\alpha)S\}\right\},\\
E_{n+1}(t) &= E_n(t) + \mathscr{L}^{-1}\left\{\frac{1}{S^a}\mathscr{L}\{\lambda^\alpha S - (\varepsilon^\alpha + \theta^\alpha + \mu^\alpha)E\}\right\},\\
A_{n+1}(t) &= A_n(t) + \mathscr{L}^{-1}\left\{\frac{1}{S^a}\mathscr{L}\{\varepsilon^\alpha E - (\mu^\alpha + \psi^\alpha + \phi^\alpha + \kappa^\alpha)A\}\right\},\\
I_{n+1}(t) &= I_n(t) + \mathscr{L}^{-1}\left\{\frac{1}{S^a}\mathscr{L}\{\theta^\alpha E + \psi^\alpha A - (\mu^\alpha + \delta^\alpha + \omega^\alpha)I\}\right\},\\
H_{n+1}(t) &= H_n(t) + \mathscr{L}^{-1}\left\{\frac{1}{S^a}\mathscr{L}\{\phi^\alpha A + \omega^\alpha I - (\mu^\alpha + \delta^\alpha + \rho^\alpha)H\}\right\},\\
R_{n+1}(t) &= R_n(t) + \mathscr{L}^{-1}\left\{\frac{1}{S^a}\mathscr{L}\{\kappa^\alpha A + \rho^\alpha H - \mu^\alpha R\}\right\}.
\end{aligned}
\tag{36}
$$

Assuming $\mathscr{X}$ is a self-map, the following results are derived:

$$
\begin{aligned}
\mathscr{X}[S_n(t)] &= S_{n+1}(t) &&= S_n(t) + \mathscr{L}^{-1}\left\{\tfrac{1}{S^a}\mathscr{L}\{\Lambda^\alpha - (\lambda^\alpha + \mu^\alpha)S\}\right\},\\
\mathscr{X}[E_n(t)] &= E_{n+1}(t) &&= E_n(t) + \mathscr{L}^{-1}\left\{\tfrac{1}{S^a}\mathscr{L}\{\lambda^\alpha S - (\varepsilon^\alpha + \theta^\alpha + \mu^\alpha)E\}\right\},\\
\mathscr{X}[A_n(t)] &= A_{n+1}(t) &&= A_n(t) + \mathscr{L}^{-1}\left\{\tfrac{1}{S^a}\mathscr{L}\{\varepsilon^\alpha E - (\mu^\alpha + \psi^\alpha + \phi^\alpha + \kappa^\alpha)A\}\right\},\\
\mathscr{X}[I_n(t)] &= I_{n+1}(t) &&= I_n(t) + \mathscr{L}^{-1}\left\{\tfrac{1}{S^a}\mathscr{L}\{\theta^\alpha E + \psi^\alpha A - (\mu^\alpha + \delta^\alpha + \omega^\alpha)I\}\right\},\\
\mathscr{X}[H_n(t)] &= H_{n+1}(t) &&= H_n(t) + \mathscr{L}^{-1}\left\{\tfrac{1}{S^a}\mathscr{L}\{\phi^\alpha A + \omega^\alpha I - (\mu^\alpha + \delta^\alpha + \rho^\alpha)H\}\right\},\\
\mathscr{X}[R_n(t)] &= R_{n+1}(t) &&= R_n(t) + \mathscr{L}^{-1}\left\{\tfrac{1}{S^a}\mathscr{L}\{\kappa^\alpha A + \rho^\alpha H - \mu^\alpha R\}\right\}.
\end{aligned}
\tag{37}
$$

The map $\mathscr{X}$ is considered stable if the following conditions are met:

$$
\begin{aligned}
&\{1 - \Lambda^\alpha - (\lambda^\alpha + \mu^\alpha)f_1\} < 1,\\
&\{1 - \lambda^\alpha f_1 - (\varepsilon^\alpha + \theta^\alpha + \mu^\alpha)f_2\} < 1,\\
&\{1 - \varepsilon^\alpha f_2 - (\mu^\alpha + \psi^\alpha + \phi^\alpha + \kappa^\alpha)f_3\} < 1,\\
&\{1 - \theta^\alpha f_2 + \psi^\alpha f_3 - (\mu^\alpha + \delta^\alpha + \omega^\alpha)f_4\} < 1,\\
&\{1 - \phi^\alpha f_3 + \omega^\alpha f_4 - (\mu^\alpha + \delta^\alpha + \rho^\alpha)f_5\} < 1,\\
&\{1 - \kappa^\alpha f_3 + \rho^\alpha f_5 - \mu^\alpha f_6\} < 1.
\end{aligned}
\tag{38}
$$

Proof:

By analysing the map $\mathscr{X}$ around a fixed point, we obtain the following equations:

$$
\begin{aligned}
\mathscr{X}[S_n(t)] - \mathscr{X}[S_m(t)] &= S_n(t) - S_m(t),\\
\mathscr{X}[E_n(t)] - \mathscr{X}[E_m(t)] &= E_n(t) - E_m(t),\\
\mathscr{X}[A_n(t)] - \mathscr{X}[A_m(t)] &= A_n(t) - A_m(t),\\
\mathscr{X}[I_n(t)] - \mathscr{X}[I_m(t)] &= I_n(t) - I_m(t),\\
\mathscr{X}[H_n(t)] - \mathscr{X}[H_m(t)] &= H_n(t) - H_m(t),\\
\mathscr{X}[R_n(t)] - \mathscr{X}[R_m(t)] &= R_n(t) - R_m(t).
\end{aligned}
\tag{39}
$$

As $\|z_{n+1} - x(X^*, z_n)\|$ approaches zero, $\|y_n - y_m\|$ converges, indicating stability. This concludes the proof.

5 Results and Discussion

In this section, we analyse the results of the fractional-order model applied to various dynamics of COVID-19 transmission and recovery. We present and discuss the graphical results and their implications on the basis of the variation in model parameters.

5.1 Crossover effect analysis

Figures 5a to 5f illustrate a notable crossover effect in the dynamics of the system. Specifically, Figures 5a, 5b and 5f exhibit this effect when the fractional order is varied. However, Figures 5c, 5d and 5e demonstrate that altering the fractional order does not always produce a crossover effect.

5.2 Impact of transmission rate variation

In Figure 6, we examined the fractional dynamics with a fractional order of $\alpha = 0.8$ of basic reproduction number $\mathscr{R}_0 = 1.9843$, the system shows distinct behaviour. When the COVID-19 transmission rate increases, Figure 6a reveals an increase in the number of people with acute COVID-19 infection. This figure also illustrates a crossover effect, where changes in transmission rates lead to significant changes in infection dynamics.

Similarly, Figure 6b shows that an increase in the COVID-19 transmission rate results in a higher number of exposed individuals, with a noticeable crossover effect observed. Figure 6c highlights that as the transmission rate increases, the number of hospitalised individuals also increases, accompanied by a crossover effect. Figure 6d shows that the number of infected individuals increases over time with increasing transmission rates. In contrast, Figure 6e reveals an opposite trend for susceptible individuals, where the number of susceptible individuals decreases as transmission rates increase. This behaviour underscores the importance of observing the dynamics of the population as the fractional order α varies. Our result here is more accurate and realistic than the results of [11, 14]

*5.3 Dynamics of recovery rate of (**A**) variation*

Figure 7 presents the dynamics of the system when the recovery rate of acutely infected individuals is varied in fractional order $\alpha = 0.8$. As shown in Figures 7a and 7b, an increase in the recovery rate of **A** results in a decrease in the number of acutely infected and hospitalised individuals. On the other hand, Figures 7c, and 7d show that an increase in the COVID-19 recovery rate leads to an increase in the number of infected and recovered individuals, respectively, illustrating a direct relationship. Our result here agrees with the results of [39, 41]

5.4 Effects of hospitalisation rate variation

The dynamics of the system with respect to varying the hospitalisation rate of infected individuals, **I**, is illustrated in Figure 8. Figure 8a shows that an increase in the hospitalisation rate of I is correlated with a decrease in the population of acutely infected individuals over time. However, Figures 8b show that increasing the hospitalisation rate of acute COVID-19 infection leads to an increase in the number of hospitalised individuals. This result agreed with the results of [55, 56, 57]

*5.5 Movement rate from (**A**) to (**I**) variation analysis*

Finally, Figure 9 explores the impact of varying the movement rate from **A** to **I** on fractional dynamics with $\alpha = 0.8$. The results indicate that changes in movement rate positively affect acutely infected individuals with COVID-19. However, this variation has a detrimental effect on exposed, hospitalised and infected compartments.

6 Conclusion

The study underscores the importance of using fractional-order models to capture the nuanced dynamics of COVID-19 transmission. By examining the effects of varying fractional orders, it becomes evident that these models provide deeper insights into how changes in disease parameters influence different stages of infection, including the number of exposed, infected, and hospitalised individuals. Our results demonstrate that the presence of crossover effects under different conditions highlights the need to choose appropriate fractional orders to accurately reflect epidemic behaviours. Furthermore, increased transmission rates are associated with higher levels of acute infections and hospitalisations, underscoring the importance of effective transmission control measures to mitigate the strain on healthcare systems.

Our findings suggest that fractional derivatives improve the alignment between modelled trajectories and observed real-world data compared to classical models, particularly in capturing delayed peaks and extended tails in infection curves. Incorporating memory effects improves predictions for long-term behaviour, aligning with observations from other infectious diseases with similar dynamics, such as influenza or measles. However, a few limitations are acknowledged. The model assumes a homogeneous population and constant parameter values, with no vertical transmissions, which may not fully capture the complexities of real-world epidemics. Furthermore, the computational complexity of fractional derivatives may pose challenges for broader applications, particularly in large-scale simulations or real-time policy-making contexts.

Future research should address these shortcomings by exploring more complex or heterogeneous population structures to improve realism, investigating adaptive or time-varying parameters to reflect changing dynamics, such as vaccination rates or public health interventions, and, moreover, developing efficient numerical methods to enhance the computational feasibility of fractional models for large-scale use. Furthermore, comparisons with a wider range of fractional-order and integer-order models could provide deeper insights into the strengths and limitations of the proposed approach. Incorporating real-world datasets from diverse contexts would enhance the generalisability and practical utility of the model. Despite these limitations, the findings underscore the potential of fractional derivatives to advance infectious disease modelling. By capturing memory effects and complex temporal dynamics, the approach offers valuable tools to understand and manage future outbreaks.

In addition, the findings suggest that higher recovery rates can reduce the incidence of acute infections, which points to the value of improved recovery strategies in managing disease progression. Variations in hospitalisation rates also affect the number of individuals hospitalised or infected, indicating that healthcare planning must account for these dynamics. The impact of movement rates between the infection and hospitalisation compartments shows how different factors can positively or negatively influence disease outcomes. In general, this research highlights the utility of fractional-order models for developing informed public health policies, emphasizing the need for precise parameter adjustments to optimize disease management strategies. Memory effects contribute to a deeper understanding of infectious disease dynamics while enhancing projection reliability.

Conflict of interest

The author declares no conflict of interest.

Data Availability Statement

The data supporting the findings of this study were sourced from the existing literature, specifically presented in Table 3.

References

[1] M.K. Ibrahim, M. Said, S. M. El-Sedfy, M. Khaled, A. Ibrahim, N. Abdellah and N. Khaled, Mathematical modelling of fractional-order COVID-19 pandemic with memory effect: a review, *MSA University Engineering Journal* **2**(2), 1–14 (2023).

[2] H. Habenom, D. L. Suthar, D. Baleanu and S. D. Purohit, Modeling and Analysis on the Transmission of COVID-19 Pandemic in Ethiopia, *Alexandria Engineering Journal* **(61)**, 5323–5342 (2022).

[3] B. Ivorra, M. R. Ferrendez, M. Vela-Perez, and A. M. Ramos, Mathematical modeling of the spread of the coronavirus disease 2019 (COVID-19) taking into account the undetected infections. The case of China, *Communications in Nonlinear Science and Numerical Simulation* **88**, 105303 (2020).

[4] A. R. J. Mumbu and A. K. Hugo, Mathematical modelling on COVID-19 transmission impacts with preventive measures: a case study of Tanzania, *Journal of Biological Dynamics* **14**, 748–766 (2020).

[5] P. A. Naik, M. Yavuz, S. Qureshi, J. Zu and S. Townley, Modeling and analysis of COVID-19 epidemics with treatment in fractional derivatives using real data from Pakistan, *The European Physical Journal Plus* **135**, 1–42 (2020).
[6] A.Abidemi, J. O. Akanni. Dynamics of illicit drug use and banditry population with optimal control strategies and cost-effectiveness analysis. *Comp. Appl. Math.* **41**, 53 (2022). https://doi.org/10.1007/s40314-022-01760-2.
[7] N. Chen, M. Zhou, X. Dong, J. Qu, F. Gong, Y. Han and L. Zhang, Epidemiological and clinical characteristics of 99 cases of new coronavirus pneumonia in 2019 in Wuhan, China: a descriptive study, *The lancet* **395**, 507–513.
[8] D. S. Hui, E. I. Azhar, T. A. Madani, F. Ntoumi, R. Kock, O. Dar and E. Petersen, The continuing 2019-nCoV epidemic threat of novel coronaviruses to global health - The latest 2019novel coronavirus outbreak in Wuhan, China, *International journal of infectious diseases* **91** , 264–266 (2020).
[9] T. Khan, R. Ullah, A. Yousef, G. Zaman, Q. M. Al-Mdallal and Y. Alraey, Modeling and dynamics of the fractional order SARS-CoV-2 epidemiological model, *Complexity* **2022**, (2022).
[10] Q. Lin, S. Zhao, D. Gao, Y. Lou, S. Yang, S. S. Musa, and D. He, A conceptual model for the 2019 coronavirus disease outbreak (COVID-19) in Wuhan, China with individual reaction and governmental action, *International Journal of Infectious Diseases* **93**, 211–216 (2020).
[11] S. Noeiaghdam, S. Micula, and J. J. Nieto, A novel technique to control the accuracy of a nonlinear fractional order model of COVID-19: application of the CESTAC method and the CADNA Library, *Mathematics* **9**, 1321 (2021).
[12] A. Abidemi, J.O. Akanni, O.D. Makinde. A non-linear mathematical model for analysing the impact of COVID-19 disease on higher education in developing countries, *Healthcare Analytics*, **3**, 2023
[13] M. Garcia, N. Lipskiy, J. Tyson, R. Watkins, E. S. Esser and T. Kinley, Centers for Disease Control and Prevention 2019 novel coronavirus disease (COVID-19) information management: addressing national health-care and public health needs for standardized data definitions and codified vocabulary for data exchange, *J Am Med Inform Assoc.* **27**, 1476â€“-1487 (2020). https://doi.org/10.1093/jamia/ocaa141.
[14] I. Ahmed, I. A. Baba, A. Yusuf, P. Kumam and W. Kumam, Analysis of Caputo fractional-order model for COVID-19 with lockdown, *Advances in Difference Equations* **2020**, 394 (2020).
[15] W. Adel, Y. A. Amer, E. S. M. Youssef and A. M. S. Mahdy, Mathematical analysis and simulations for a Caputo-Fabrizio fractional COVID-19 model, *Partial Differential Equations in Applied Mathematics* **8**, 100558 (2023).
[16] W.-M. Liu, H. W. Hethcote, and S.A. Levin, Dynamical behavior of epidemiological models with nonlinear incidence rates, *J. Math. Biol.* **25** (4), 359â€“380 (1987).
[17] F. Brauer, The Kermack-Mckendrick epidemic model revisited, *Math. Biosci.* **198** (2), 119â€“-131 (2005).
[18] O. Sharomi, C. N. Podder, A. B. Gumel and B. Song, Mathematical analysis of the transmission dynamics of HIV/TB coinfection in the presence of treatment, *Math. Biosci. Eng.*, **5**(1), 145 (2008).
[19] C. Castillo-Chavez and B. Song, Dynamical models of tuberculosis and their applications,*Math. Biosci. Eng.*, **1** (2), 361 (2004).
[20] N.R. Sasmita, M. Ikhwan, S. Suyanto and V. Chongsuvivatwong, Optimal control on a mathematical model to pattern the progression of coronavirus disease 2019 (COVID-19) in indonesia, *Global Health Res., Policy* **5** (1), 1â€“-12 (2020).
[21] G. Giordano, F. Blanchini, R. Bruno, P. Colaneri, A. Di Filippo, A. Di Matteo and M. Colaneri, Modelling the COVID-19 epidemic and implementation of population-wide interventions in italy, *Nat. Med.*, **2020** 1-â€“6 (2020).
[22] X. Rong, L. Yang, H. Chu and M. Fan, Effect of delay in diagnosis on transmission of COVID-19, *Math. Biosci. Eng.* **17**(3), 2725-â€“2740 (2020).
[23] A.-R. J. Mumbu and A. K. Hugo, Mathematical modelling on COVID-19 transmission impacts with preventive measures: a case study of tanzania, *J. Biol. Dyn.* **14** (1), 748â€“-766 (2020).
[24] E. B. Postnikov, Estimation of COVID-19 dynamics â€ on a back-of-envelopeâ€ : Does the simplest SIR model provide quantitative parameters and predictions?, *Chaos Solitons Fract.* **135**, 109841 (2020),
[25] S. S. Musa, S. Qureshi, S. Zhao, A. Yusuf, U. T. Mustapha and D. He, Mathematical modeling of COVID-19 epidemic with effect of awareness programs, *Infectious Dis. Model.* **6**, 448â€“-460 (2021).
[26] Z. Memon, S. Qureshi and B. R. Memon, Assessing the role of quarantine and isolation as control strategies for COVID-19 outbreak: A case study,*Chaos Solitons Fract.* **144**, 110655 (2021).
[27] K. Shah, T. Abdeljawad, I. Mahariq and F. Jarad, Qualitative analysis of a mathematical model in the time of COVID-19, *BioMed Res. Int.* **2020**, 5098598 (2020).
[28] A. S. Shaikh, I. N. Shaikh and K. S. Nisar, A mathematical model of COVID-19 using fractional derivative: Outbreak in India with dynamics of transmission and control, *Adv. Differ. Equ.* **2020**, 373 (2020).
[29] M. S. Abdo, K. Shah, H. A. Wahash and S. K. Panchal, On a comprehensive model of the novel coronavirus (COVID-19) under Mittag-Leffler derivative, *Chaos Solitons Fractals* **135**, 109867 (2020).
[30] A. Kilbas, H. Srivastava and J. Trujillo, Theory and Applications of Fractional Differential Equations. *North-Holland Mathematics Studies* **204**, (2006).
[31] D. P. Smethurst and H. C. Williams, Are hospital waiting lists self-regulating? *Nature* **410**(6829), 652â€“653 (2001).
[32] M. M. Meerschaert and A. Sikorskii, *Stochastic Models for Fractional Calculus*, 43. de Gruyter, Berlin, (2011).
[33] J. O. Akanni, F. Fatmawati, C. W. Chukwu. On the fractional-order modeling of COVID-19 dynamics in a population with limited resources, *Commun. Math. Biol. Neurosci.*, **2023** (2023).
[34] K. Shah, M. A. Alqudah, F. Jarad and T. Abdeljawad, Semi-analytical study of Pine Wilt disease model with convex rate under Caputoâ€“Fabrizio fractional order derivative, *Chaos Solitons Fractals* **135**, 109754 (2020).

[35] J. Gomez-Aguilar, T. Cordova-Fraga, T. Abdeljawad, A. Khan and H. Khan, Analysis of fractal-fractional malaria transmission model, *Fractals*, (2020).
[36] K. Shah, F. Jarad and T. Abdeljawad, On a nonlinear fractional order model of Dengue fever disease under Caputoâ€“Fabrizio derivative, *Alex. Eng. J.*, (2020).
[37] M. Yousaf, S. Zahir, M. Riaz, S. M. Hussain and K. Shah, Statistical analysis of forecasting COVID-19 for upcoming month in Pakistan, *Chaos Solitons Fractals* **138**, 109926 (2020).
[38] C. T. Codec o, Endangered and epidemic dynamics of cholera: the role of the aquatic reservoir, *BMC Infectious Dis.* **1** (1), (2001).
[39] M. Javidi and B. Ahmad, A study of a fractional-order cholera model, *Appl. Math. Inform. Sci.* **8** (5), 2195 (2014).
[40] C. Vargas-De-Leon, Volterra-type Lyapunov functions for fractional-order epidemic systems, *Commun. Nonlinear Sci. Numer. Simul.* **24** (1â€“3), 75â€-85 (2015).
[41] E. Demirci, A fractional order model for obesity epidemic in a non-constant population, *Adv. Differ. Eqs.* **2017** (1), 79 (2017).
[42] N. OZalp and E. Demirci, A fractional-order SEIR model with vertical transmission, *Math. Comput. Model* **54** (1â€“2), 1â€“6 (2011).
[43] J. O. Akanni. Mathematical assessment of the role of illicit drug use on terrorism spread dynamics. *J. Appl. Math. Comput.* **68**, 3873â€“3900 (2022).
[44] S. Qureshi, Periodic dynamics of rubella epidemic under standard and fractional caputo operators with real data from Pakistan, *Math. Comput. Simul.* **178**, 151â€-165 (2020),.
[45] J. V. L. Chew, A. Sunarto, J. Sulaiman and M. F. Asli, Fractional Newton Explicit Group Method for Time-Fractional Nonlinear Porous Medium Equations, *Progr. Fract. Differ. Appl.* **10**(3), 391–398 (2024).
[46] D. Baleanu, A. Jajarmi, S. S. Sajjadi and D. Mozyrska, A new fractional model and optimal control of a tumor-immune surveillance with non-singular derivative operator, *Chaos: An Interdisciplinary Journal of Nonlinear Science* **29**(8), 083127 (2019).
[47] D. Baleanu, P. Shekari, L. Torkzadeh, H. Ranjbar, A. Jajarmi and K. Nouri, Stability analysis and system properties of Nipah virus transmission: A fractional calculus case study, *Chaos, Solitons & Fractals* **166**, 112990 (2023).
[48] O. Defterli, D. Baleanu, A. Jajarmi, S. S. Sajjadi, N. Alshaikh and J. H. Asad, Fractional treatment: an accelerated mass-spring system, *Romanian Reports in Physics* **74** (4), 122 (2022).
[49] P. Kumar and S. Qureshi, Laplace-Carson integral transform for exact solutions of noninteger-order initial value problems with the Caputo operator, *J. Appl. Math. Comput. Mech.* **19** (1), 57â€-66 (2020).
[50] P. Perdikaris and G. E. Karniadakis, Fractional-order viscoelasticity in one-dimensional blood flow models, *Ann. Biomed. Eng.* **42** (5), 1012â€-1023 (2014).
[51] C. M. Pinto and A. R. Carvalho, The role of synaptic transmission in a HIV model with memory, *Appl. Math. Comput.* **292**, 76â€–95 (2017).
[52] M. Yavuz and N. Ozdemir, A different approach to the European option pricing model with new fractional operator, *Math. Model. Nat. Phenomena* **13** (1), 12 (2018).
[53] I. A. Baba and B. A. Nasidi, Fractional order epidemic model for the dynamics of novel COVID-19, *Alexandria Eng. J.* **60** (1), 537â€548 (2021).
[54] M. A. Bahloul, A. Chahid and T. M. Laleg-Kirati, Fractional-order SEIQRDP model for simulating the dynamics of COVID-19 epidemic, *IEEE Open J. Eng. Med. Biol.* **1**, 249â€-256 (2020),
[55] S. Ahmad, A. Ullah, Q.M. Al-Mdallal, H. Khan, K. Shah and A. Khan, Fractional order mathematical modeling of COVID-19 transmission, *Chaos Solitons Fract.* **139**, 110256 (2020).
[56] I. Ahmed, I.A. Baba, A. Yusuf, P. Kumam and W. Kumam, Analysis of caputo fractional-order model for COVID-19 with lockdown, *Adv. Differ. Eqs.* **2020** (1), 1â€-14 (2020).
[57] Z. Zhang, A. Zeb, O. F. Egbelowo and V. S. Erturk, Dynamics of a fractional-order mathematical model for covid-19 epidemic, *Adv. Differ. Eqs.* **2020** (1), 1â€-16 (2020).
[58] I. Owusu-Mensah, L. Akinyemi, B. Oduro and O. S. Iyiola, A fractional order approach to modeling and simulations of the novel COVID-19, *Adv. Differ. Eqs.* **2020** (1), 1â€-21 (2020).
[59] N. H. Tuan, H. Mohammadi and S. Rezapour, A mathematical model for COVID-19 transmission by using the Caputo fractional derivative, *Chaos Solitons Fract.* **140**, 110107 (2020).
[60] S. O. Akindeinde, E. Okyere, A. O. Adewumi, R. S. Lebelo, O. O. Fabelurin and S. E. Moore, Caputo fractional-order SEIRP model for COVID-19 Pandemic, *Alexandria Engineering Journal* **61**, 829â€-845 (2022).
[61] S. Ajao, I. Olopade, T. Akinwumi, S. Adewale and A. Adesanya, Understanding the transmission dynamics and control of HIV infection: A mathematical model approach, *Journal of the Nigerian Society of Physical Sciences* **5**(2), 1389 (2023).
[62] P. van den Driessche and J. Watmough, Reproduction numbers and sub-threshold endemic equilibria for compartmental models of disease transmission, *Mathematical Biosciences* **180**, 29â€-48 (2002).
[63] C. Castillo-Chavez, Z. Feng and W. Huang, On the computation of R_o and its role on global stability. In: C. Castillo-Chavez, P. van den Driessche, D. Kirschner D and A-A. Yakubu (eds.) *Mathematical Approaches for Emerging and Re-emerging Infectious Diseases: An Introduction.* Berlin: Springer-Verlag, **2002**, 229–250.(2002).
[64] J. P. LaSalle, *The stability of Dynamical Systems*, Regional Conference Series in Applied Mathematics, SIAM, Philadelphia, (1976)
[65] D. Okuonghae and A. Omame, Analysis of a mathematical model for COVID-19 population dynamics in Lagos, Nigeria, *Chaos Solitons Fractals* **139**, 110032 (2020). https://doi:10.1016/j.chaos.2020.110032.
[66] S. I. Oke, M. I. Ekum, O. J. Akintande, M. O. Adeniyi, T. A. Adekiya, O. J. Achadu, M. B. Matadi, O. S. Iyiola and S. O. Salawu, Optimal control of the coronavirus pandemic with both pharmaceutical and non-pharmaceutical interventions, *Int. J. Dynam. Control* **2023**, (2023). https://doi.org/10.1007/s40435-022-01112-2.

[67] A. Kouidere, O. Balatif and M. Rachik, Cost-effectiveness of a mathematical modeling with optimal control approach of spread of COVID-19 pandemic: A case study in Peru, *Chaos, Solitons & Fractals* X, *10*, 100090 (2023). https://doi.org/10.1016/j.csfx.2022.100090

[68] J. N. Paul, I. S. Mbalawata, S. S. Mirau and L. Masandawa, Mathematical modeling of vaccination as a control measure of stress to fight COVID-19 infections, *Chaos, Solitons & Fractals* **166**, 112920 (2023). https://doi.org/10.1016/j.chaos.2022.112920

[69] S. M. Garba, J. M. Lubuma and B. Tsanou, Modeling the transmission dynamics of the COVID-19 Pandemic in South Africa, *Math Biosci.* **328**, 108441 (2020). https://doi:10.1016/j.mbs.2020.108441

[70] B. Tang, N. L. Bragazzi, Q. Li, S. Tang, Y. Xiao and J. Wu, An updated estimation of the risk of transmission of the novel coronavirus (2019-nCov). Infectious Disease Modelling, 5, 248–255 (2020). https://doi.org/10.1016/j.idm.2020.02.001

[71] S. Cauchemez, C. Fraser, M. D. Van Kerkhove, C. A. Donnelly, S. Riley, A. Rambaut, V. Enouf, S. van der Werf, and N. M. Ferguson, Middle East respiratory syndrome coronavirus: quantification of the extent of the epidemic, surveillance biases, and transmissibility, *Lancet Infect Dis.* **14** (1), 50–56 (2014). https://doi:10.1016/S1473-3099(13)70304-9.

[72] B. Yang, Z. Yu, and Y. Cai, The impact of vaccination on the spread of COVID-19: Studying by a mathematical model. *Physica A* **590**, 26717 (2022). https://doi:10.1016/j.physa.2021.126717.

[73] N. M. Ferguson, D. J. Laydon, G. N. Gilani, N. Imai, K. E. Ainslie, M. Baguelin, S. Bhatia, A. Boonyasiri, Z. C. Perez, G. Cuomo-Dannenburg, A. Dighe, I. Dorigatti, H. Fu, K. A. Gaythorpe, W. Green, A. Hamlet, W. Hinsley, L. C. Okell, S. V. Elsland, H. A. Thompson, R. Verity, E. M. Volz, H. Wang, Y. Wang, P. G. Walker, C. E Walters, P. Winskill, C. Whittaker, C. A. Donnelly, S. Riley and A. C. Ghani, *Report 9: Impact of non-pharmaceutical interventions (NPIs) to reduce COVID19 mortality and healthcare demand*. Imperial College London. (2020). https://doi.org/10.25561/77482

[74] I. Podlubny, *Fractional Differential Equations*, Mathematics in Science and Engineering, **198**(2),289, Academic Press, San Diego, California, USA, (2000).

[75] Z. M. Odibat and N. T. Shawagfeh, Generalized Taylor's formula. *Applied Mathematics Computation* **186**(1), 286–293 (2007).

[76] S. Mangal, O. Misra and J. Dhar, Fractional-order deterministic epidemic model for the spread and control of HIV/AIDs with special reference to Mexico and India. *Mathematics Computation Simulation* **210**(82), 82–102 (2023).